1152 *Inorg. Chem.* **2010**, *49*, 1152–1157
DOI: 10.1021/ic9020096

Inorganic Chemistry
Article

Interconversion of Perovskite and Fluorite Structures in Ce−Sc−O System

Rakesh Shukla,[†] Ashok Arya,[‡] and Avesh K. Tyagi*[,†]

[†]*Chemistry Division and* [‡]*Materials Science Division, Bhabha Atomic Research Centre, Mumbai 400 085, India*

Received October 12, 2009

$CeScO_3$ was synthesized by a two-step synthesis route involving a combustion method followed by vacuum heating at 1100 °C in the presence of Zr sponge which acts as an oxygen getter. The compound was characterized by various techniques such as X-ray diffraction (XRD), high temperature XRD, thermogravimetry, diffuse reflectance (DR)-UV visible spectrophotometry, and Raman spectroscopy. Fluorite-type (F-type) solid solution with composition $Ce_{0.5}Sc_{0.5}O_{1.75}$ was observed as an intermediate during the synthesis of $CeScO_3$. Only by mere redox reaction was a reversible transformation between fluorite-type structure and perovskites structure observed. $CeScO_3$ was found as semiconducting oxide with band gap of 3.2 eV arising mainly between O p states in the valence band and Sc d and Ce d states in the conduction band with small contributions coming from Ce f and Sc p states. First-principles potential plane-wave-based calculations were performed for the band gap and its origin in $CeScO_3$. Photoluminescence measurement showed that $CeScO_3$ is a potential host material giving broad blue emission. This was further confirmed by demonstrating $CeScO_3$ doped with 2 mol % Tb^{3+} compound as an efficient green light emitter.

Introduction

Rare-earth scandates with chemical formula $REScO_3$ (RE = rare-earths) are known to have high dielectric constant and large band gap values between 5 and 6 eV.[1] They are candidate substrates for epitaxial growth of perovskite and perovskite-related films.[2−5] These rare-earth scandates have pseudocubic lattice constants in the range of 3.93−4.05 Å. At room temperature, $REScO_3$ (RE = La to Ho) have orthorhombic $GdFeO_3$ crystal structure (space group *Pnma*).[6−12] Among the rare-earth scandates, cerium scandate is scantily reported as the presence of Ce^{3+} ion at A-site of the perovskite lattice makes the preparation of $CeScO_3$ quite unfavorable. Since the tolerance factor (t = 0.90) allows the crystallographic stability of this material, there is no reason that $CeScO_3$ should not form, except the lack of a suitable synthesis route. Perhaps this may be the reason why there is only one report on the preparation of $CeScO_3$ wherein an arc-melting method involving CeO_2, Sc_2O_3, and Sc metal was used.[13] In this manuscript, we report a chemical route for the preparation of $CeScO_3$. The properties of this compound were further studied by measuring the band gap and optical properties, as discussed subsequently.

2. Experimental Procedure

2.1. Synthesis. In order to prepare $CeScO_3$ and $CeScO_3$ doped with 2 mol % of Tb^{3+} ion, the glycine−nitrate combustion reaction was performed with respective metal nitrates in a fuel- deficient ratio[14] (1:1.5) to obtain the nanopowders. The as-synthesized powders were calcined at 600 °C for 1 h in air to remove the volatile carbonaceous impurities, if any. These powders were pelletized, wrapped in a tantalum foil, and vacuum-sealed in a quartz tube in the presence of a Zr sponge

*To whom correspondence should be addressed. E-mail: aktyagi@barc.gov.in. Fax: +91-22-25505151. Phone: +91-22-25595330.

(1) Christen, H. M.; Jellison, G. E.; Ohkubo, I.; Huang, S.; Reeves, M. E.; Cicerrella, E.; Freeouf, J. L.; Jia, Y.; Schlom, D. G. *Appl. Phys. Lett.* **2006**, *88*, 262906.
(2) Schubert, J.; Trithaveesak, O.; Petraru, A.; Jia, C. L.; Uecker, R.; Reiche, P.; Schlom, D. G. *Appl. Phys. Lett.* **2003**, *82*, 3460.
(3) Karimoto, S.-I.; Naito, M. *Appl. Phys. Lett.* **2004**, *84*, 2136.
(4) Landolt-Börnstein. Numerical Data and Functional Relationships in Science and Technology. In *Crystal structure data of inorganic compounds*; Hellwege, K.-H., Hellwege, A. M., Eds.; New Series-Group III; Springer-Verlag: Berlin, 1976; Vol. *7*, pp 11−13.
(5) Biegalski, M. D.; Haeni, J. H.; S. McKinstry, T.; Schlom, D. G. *J. Mater. Res.* **2005**, *20*, 952.
(6) Badie, J. M. *High Temp. High Press.* **1970**, *2*, 309.
(7) Amanyan, S. N.; Antipov, E. V.; Antonov, V. A.; Arsen'ev, P. A.; Bagdasarov, Kh.S.; Kevorkov, A. M.; Kovba, L. M.; Rakhmatuli, A. V. *Russ. J. Inorg. Chem.* **1987**, *32*, 2087.
(8) *Space Group Symmetry, International Tables for Crystallography*, 5th ed.; Kluwer: Dordrecht, The Netherlands, 2002; Vol. *A*.
(9) Megaw, H. D. *Crystal Structures: A Working Approach*; W. B. Saunders Co.: Philadelphia, PA, 1973.
(10) Eom, C. B.; Cava, R. J.; Fleming, R. M.; Phillips, J. M.; van Dover, R. B.; Marshall, J. H.; Hsu, J. W. P.; Krajewski, J. J.; Peck, W. F., Jr. *Science* **1992**, *258*, 1766.
(11) McClune, W.F., Mrose, M.E., Post, B., Weissmann, S., McMurdie, H.F., Evans, E., Wong-Ng, W., Eds. *Powder Diffraction File Card 27-220 sets 27−28*; International Centre for Diffraction Data: Swarthmore, PA, **1986**; p 78.
(12) McClune, W. F., Mrose, M. E., Post, B., Weissmann, S., McMurdie, H. F., Evans, E., Wong-Ng, W., Eds. *Powder Diffraction File Card 27-204, sets 27−28*; International Centre for Diffraction Data: Swarthmore, PA, **1986**; p .72
(13) Greedan, J. E.; Seto, K. *Mater. Res. Bull.* **1981**, *16*, 1479.
(14) Bedekar, V.; Shukla, R.; Tyagi, A. K. *Nanotechnology*. **2007**, *18*, 155706.

 Published on Web 12/30/2009

(oxygen getter) and heated at 1100 °C for 24 h to obtain phase pure $CeScO_3$. $Ce_{0.5}Sc_{0.5}O_{1.75}$ is light yellow in color while $CeScO_3$ is white in color when freshly prepared which slowly with time turns to a dirty greenish color.

2.2. Structural Characterization and Property Measurements. X-ray diffraction studies were carried on the sample for the phase identification, using monochromatized Cu Kα radiation on X'pert PRO XRD unit. Silicon was used as an external standard. The high temperature X-ray diffraction (HT-XRD) patterns of the sample were recorded using an X'pert PRO XRD unit fitted with an Anton Parr high temperature attachment. A platinum heater was used as the stage for the sample. The temperature was controlled with an accuracy of ±1 K using Eurotherm temperature controller. The XRD patterns were recorded at various temperatures in the range of 25 to −1100 °C after holding the sample for 30 min at each desired temperature, in static air. Photoluminescence measurements were carried out on $CeScO_3$ and Tb^{3+} doped $CeScO_3$ at room temperature with a resolution of 3 nm using a Hitachi instrument (F-4500) having a 150 W Xe lamp excitation source. An approximately 20 mg sample was dispersed in 5 mL methanol prior to luminescence measurements. The optical band gap of $CeScO_3$ was measured by a diffuse reflectance (DR)-UV−visible spectrophotometer in the reflectance mode.

2.3. Theoretical Calculation. Theoretical calculations for the band gap and its origin in $CeScO_3$ were carried out by performing "projector augmented wave" (PAW) potential plane-wave-based density functional theory (DFT) calculations (see section 3.4 for details).

3. Results and Discussion

3.1. Synthesis. The combustion synthesis is one of the alternate chemical routes which have been successfully employed to prepare nanocrystalline materials. The solution combustion process is basically a redox reaction between an oxidant usually metal nitrate and a fuel like glycine, citric acid, etc.[15] The main motivation for using this preparative technique was to achieve an atomistically blended precursor containing appropriate amounts of CeO_2 and Sc_2O_3, which will facilitate the preparation of $CeScO_3$ at a later stage. The oxidizing valency of $Ce(NO_3)_3 \cdot 6H_2O$ and $Sc(NO_3)_3$ is 15− each, whereas the reducing valency of glycine is 9+, calculated by considering the valencies of individual ions, as described earlier.[14] A stoichiometric oxidant-to-fuel ratio in this case ($CeScO_3$) comes out to be 30/9 = 3.33. Earlier, it was observed in our group that due to the low exothermicity of glycine−nitrate combustion in a fuel-deficient ratio, nanopowders with better powder properties are obtained.[16] Hence, for the preparation of nanocrystalline a ceria−scandia mixture, a 55% fuel-deficient ratio comparted to a stoichiometric ratio (1:1.5) was preferred. i.e 1 mmol (0.4342 g) of $Ce(NO_3)_3 \cdot 6H_2O$ and 1 mmol (0.3030 g) of $Sc(NO_3)_3 \cdot 4H_2O$ were dissolved in 10 mL of distilled water. A 1.5 mmol (0.1125 g) portion of glycine was added to the solution. This solution on thermal dehydration autoignited with a large amount of gaseous evolution. These evolved gases dissipate the heat and in turn minimize the local sintering making the powders highly porous and frothy. Similarly, for preparation of nanocrystalline CeO_2/Sc_2O_3 individually, a 55% fuel-deficient ratio compared to the stoichiometric ratio (1:0.75) was preferred, and 1 mmol of $Ce(NO_3)_3 \cdot 6H_2O$ or $Sc(NO_3)_3 \cdot 4H_2O$ was taken along with 0.75 mmol of glycine. The powders synthesized after combustion reaction were calcined at 600 °C for 1 h in air to remove the volatile impurities, if any.

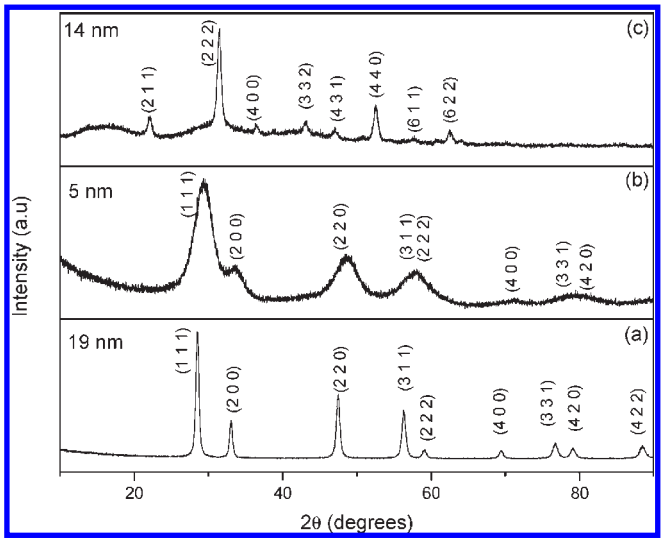

Figure 1. Indexed XRD pattern of (a) nano-CeO_2, (b) $Ce_{0.5}Sc_{0.5}O_{1.75}$ solid solution, and (c) nano-Sc_2O_3 synthesized under identical conditions.

3.2. X-ray Diffraction. The indexed powder X-ray diffraction pattern of the combustion-synthesized CeO_2, $Ce_{0.5}Sc_{0.5}O_{1.75}$, and Sc_2O_3 are shown in Figure 1. The XRD pattern of $Ce_{0.5}Sc_{0.5}O_{1.75}$ does not show peaks due to CeO_2 or Sc_2O_3. However, there is considerable shift in the XRD peaks of $Ce_{0.5}Sc_{0.5}O_{1.75}$ compared to that of CeO_2. Indexing and refinement revealed a decrease of cell parameters of nano-CeO_2 from 5.4201 (8) to 5.3409 (12) Å of $Ce_{0.5}Sc_{0.5}O_{1.75}$, which is attributed to the large difference in the ionic radii (in 8-fold coordination) of Ce^{4+} (0.90 Å) and Sc^{3+}(0.75 Å). Thus, the formation of fluorite−type (F-type) solid solution can be inferred from this observation. This result assumes further significance in view of the fact that Sc_2O_3 does not have any solubility in CeO_2 by the solid state method,[17] and to date, only one report is available for CeO_2−Sc_2O_3 solid solution wherein the authors have substituted maximum of 10 mol % Sc_2O_3 in the ceria lattice by a coprecipitation method.[18] To best of our knowledge, it is for the first time that 50 mol % solubility of Sc_2O_3 in CeO_2 has been observed. This solid solution stabilization in CeO_2−Sc_2O_3 system can be attributed to the nanonature of the sample and nonequilibrium method employed in this work. The average crystallite size of the nanocrystalline CeO_2, Sc_2O_3, and $Ce_{0.5}Sc_{0.5}O_{1.75}$ calculated from the Scherer's formula was found to be about 19, 14, and 5 nm, respectively. It can be seen from the XRD pattern that the broadening in the $Ce_{0.5}Sc_{0.5}O_{1.75}$ solid solution is comparatively more than the CeO_2 and Sc_2O_3 prepared under identical condition, this increased broadening perhaps can be attributed to incorporation of Sc^{3+} ion in the

(15) Purohit, R. D.; Sharma, B. P.; Pillai, K. T.; Tyagi, A. K. *Mater. Res. Bull.* **2001**, *36*, 2711.
(16) Bedekar, V.; Chavan, S. V.; Tyagi, A. K. *J. Mater. Res.* **2007**, *22*, 587.
(17) Grover, V.; Banerji, A.; Sengupta, P.; Tyagi, A. K. *J. Solid State Chem.* **2008**, *181*, 1930.
(18) Li, P.; Chen, I.; Penner-Hahn, J. E.; Tien, T. *J. Am. Ceram. Soc.* **1991**, *74*, 958.

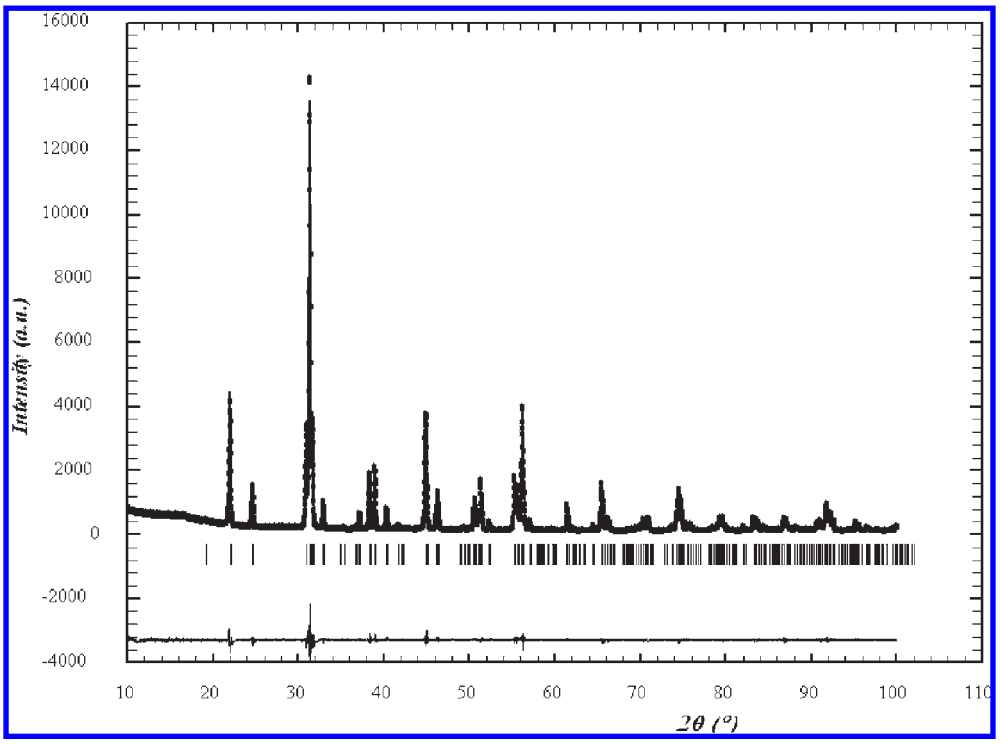

Figure 2. Rietveld refined powder XRD pattern for $CeScO_3$. (The black dot represents the observed data, and the black solid line indicates the calculated pattern. Tick marks indicate the positions of the Bragg reflections. The bottom line below the tick marks is the difference between the observed and the calculated patterns).

CeO_2 lattice. Similar observation of increased full width at half maximum (fwhm) as a function of aliovalent ion substitution was reported by us in the $Ce_{1-x}Nd_xO_{2-x/2}$ system in which all the samples were prepared under identical conditions.[19] The calcined powder was then ground and pelletized. The pellets were wrapped in tantalum foil and placed in a quartz tube containing thin pelletized zirconium metal powder. A Zr sponge was taken in about double the weight of reactants. The quartz tube was then vacuum sealed at 10^{-6} mbar pressure and heated to 1100 °C for 24 h with heating and cooling rates of 4 °C/min. During this heat treatment in the presence of Zr powder, there is a further reduction of partial pressure of O_2, which facilitates the reduction of solid solution $Ce_{0.5}Sc_{0.5}O_{1.75}$ leading to the formation of $CeScO_3$ perovskite. Tantalum foil was taken so as to avoid the direct contact of pellet and Zr sponge. In addition, the Ta metal acts as oxygen getter to an extent facilitating the reduction procedure. The Rietveld fitted XRD pattern of $CeScO_3$ is shown in Figure 2. No detectable reflections attributable to the impurities such as CeO_2, Sc_2O_3, or their solid solution were observed, indicating the single phasic nature of the product. Rietveld refinement on the XRD data of $CeScO_3$ was carried out using Fullprof-2K software package,[20] and the obtained results are given in Table 1. All the diffraction peaks for $CeScO_3$ were indexed on an orthorhombic unit cell with a = 5.7772 (1), b = 8.0473 (1), and c = 5.6429 (1) Å, which was found to be in good agreement with the reported data.[13] From the refinement analysis, not more than 0.2% of mixing of Ce and Sc was observed at the A- and B-sites of the perovskite structure.

Table 1. Typical Crystallographic and Structure Refinement Parameters for $CeScO_3$

molecular formula	$CeScO_3$
molecular weight	233.07
space group	*Pnma* (no. 62)
unit cell parameters	
a	5.7772 (1) Å
b	8.0473 (1) Å
c	5.6429 (1) Å
volume and *Z*	262.34 (0) Å^3, 4
Ce	
x	0.04603 (12)
y	0.25000 (0)
z	−0.01041 (22)
B_{iso}	0.250 (19)
Cr (*x*,*y*,*z*)	(0,0,1/2)
B_{iso}	0.732 (46)
O1	
x	0.46871 (134)
y	0.25000 (0)
z	0.10569 (145)
B_{iso}	1.112(227)
O2	
x	0.29804 (106)
y	0.05042 (82)
z	0.70594 (112)
B_{iso}	0.863 (0)
density (calculated)	5.90 g/cm^3
number of free parameters	21
profile	pseudo-Voigt
goodness-of-fit (χ^2)	1.86
R_p, R_{wp}, R_{exp} R_B, and R_F	5.52, 7.19, 5.27, 2.28, 1.84

3.3. Thermal and Optical Properties. In order to evaluate the thermal stability of the $CeScO_3$, its high temperature XRD patterns were recorded at different temperatures (RT-1100 °C-cooled RT) as shown in Figure 3. The HT-XRD data revealed the oxidation of

(19) Bedekar, V.; Tyagi, A. K. *J. Nanosci. Nanotechnol.* **2007**, *7*, 3214.
(20) Roisnel, T.; Rodriguez-Carvajal, J. *FULLPROF 2005: A Program for Rietveld, Profile Matching and Integrated Intensity Refinements for X-ray and Neutron Data*; LLB Saclay−LCSIM, Rennes, France, 2005.

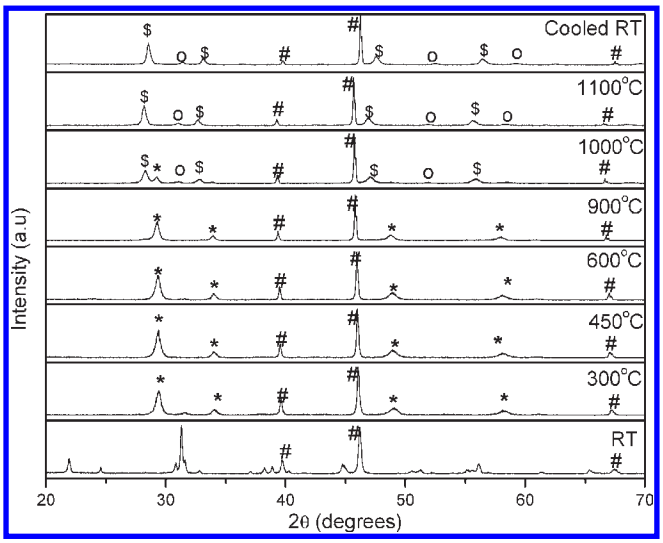

Figure 3. HT-XRD pattern of $CeScO_3$ perovskite (RT, 1100 °C, and cooled RT): (*) $Ce_{0.5}Sc_{0.5}O_{1.75}$, ($) CeO_2, (○) Sc_2O_3, (#) platinum holder peak.

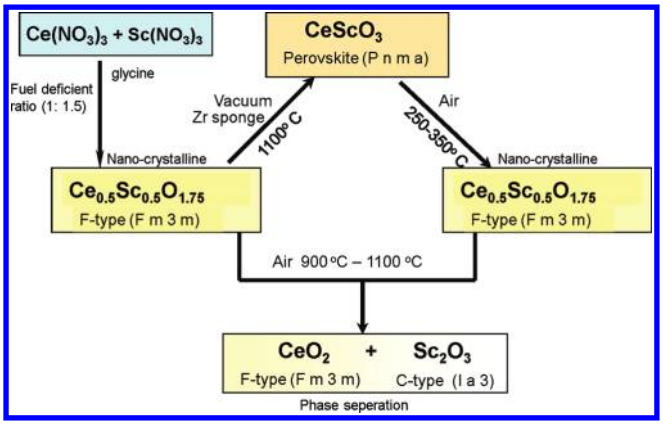

Figure 4. Phase changes brought in the system by change in conditions.

sample between 250 and 350 °C in static air resulting in transformation of $CeScO_3$ perovskite to F-type solid solution $Ce_{0.5}Sc_{0.5}O_{1.75}$. This solid solution is stable up to 900 °C in air, above which, phase separation of $CeScO_3$ to CeO_2 and Sc_2O_3 initiates. Complete phase separation is seen at around 1100 °C. These observations clearly explain why ceramic route cannot be used to prepare ceria−scandia solid solution, as $Ce_{0.5}Sc_{0.5}O_{1.75}$ is unstable above 900 °C in air. The schematic representation of phase changes brought in the system by change in conditions is shown in Figure 4.

It can be noted that only by mere redox reaction a fluorite type structure of $Ce_{0.5}Sc_{0.5}O_{1.75}$ could be transformed to perovskite structure of $CeScO_3$ and vice versa. A similar type of fluorite to perovskite transformation was observed by Brennecka et al. in PbO based thin and ultrathin films.[21] Perovskite to fluorite transformation as observed here is not a displacive type. It is a reconstructive type transformation which may be attributed to the decomposition of the perovskite structure driven by the oxidation of Ce^{3+} which leads to the formation of fluorite structure. Since the fluorite lattice is formed by

(21) Brennecka, G. L.; Parish, C. M.; Tuttle, B. A.; Brewer, L. N.; Rodriguez, M. A. *Adv. Mater.* **2008**, *20*, 1407.

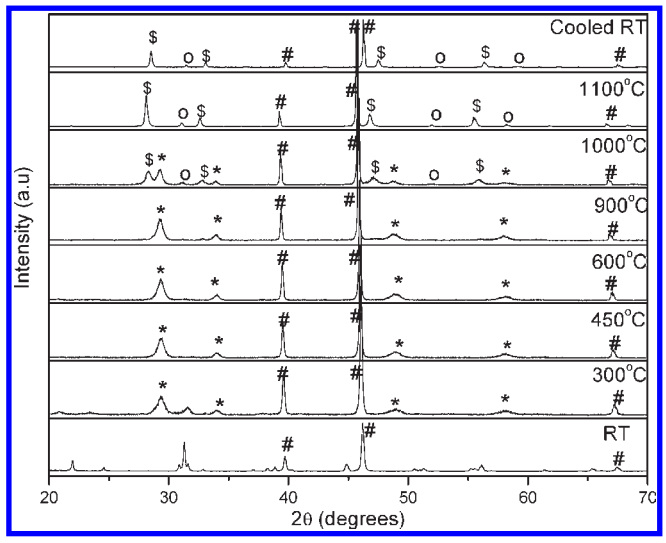

Figure 5. HT-XRD pattern of $CeScO_3$ perovskite 2nd cycle (RT, 1100 °C, and cooled RT): (*) $Ce_{0.5}Sc_{0.5}O_{1.75}$, ($) CeO_2, (○) Sc_2O_3, (#) platinum holder peak.

breaking down of the ordered perovskite lattice occurring in a local region, it leads to the formation of nanocrystalline $CeO_2-Sc_2O_3$ solid solution. This is a sort of lattice crumbling phenomenon. The formation of nanocrystalline solid solution might be an artifact of this preparation protocol nanocrystalline. The crystallite size of $Ce_{0.5}Sc_{0.5}O_{1.75}$ obtained by decomposition of $CeScO_3$ at 300 and 900 °C was found to be around 17 and 23 nm, respectively. The widths of the XRD peaks of the $Ce_{0.5}Sc_{0.5}O_{1.75}$ phase does not change much even after heating up to 900 °C to preserve the phase stability. To confirm this, the $Ce_{0.5}Sc_{0.5}O_{1.75}$ fluorite solid solution obtained by combustion was reduced to obtain $CeScO_3$ compound. $CeScO_3$ obtained (1st cycle-oxidation) was oxidized to get back the solid solution and then again reduced to get $CeScO_3$.This second time obtained $CeScO_3$ was further subjected to reoxidation in air. The second HT-XRD cycle obtained $CeScO_3$ (2nd cycle oxidation) is given in Figure 5. The crystallite size obtained after the second cycle of the reduction−oxidation cycle at 300 and 900 °C was 12 and 16 nm, respectively. From this process, it can be inferred that the solid solution remains in the nanoregime to preserve the stability of the highly concentrated $Ce_{0.5}Sc_{0.5}O_{1.75}$ solid solution.

In order to quantitatively study the thermal stability of $CeScO_3$, thermogravimetry was carried out on the sample in air. Thermogravimetric data is shown in Figure 6. It was observed that $CeScO_3$ oxidizes to $Ce_{0.5}Sc_{0.5}O_{1.75}$ over the temperature range 250−350 °C, accompanied with a weight gain of 3.45%, which is in close agreement with the theoretical value of 3.43%; corresponding to the gain of 1/2 O_2 per $CeScO_3$ molecule. The XRD pattern of the residue matches well with that of $Ce_{0.5}Sc_{0.5}O_{1.75}$ solid solution. In order to further confirm the structure of bulk ceria, nanocrystalline CeO_2, $Ce_{0.5}Sc_{0.5}O_{1.75}$, and $CeScO_3$, their Raman spectra were recorded (Figure 7). Pure ceria exhibits a sharp first-order Raman peak at 455 cm^{-1} assigned to the F_2g mode due to the symmetrical stretching of the Ce−O vibrational unit in 8-fold coordination. The shift and broadening in the peak of nanoceria from the bulk ceria (465 cm^{-1}) is due to the nanocrystalline

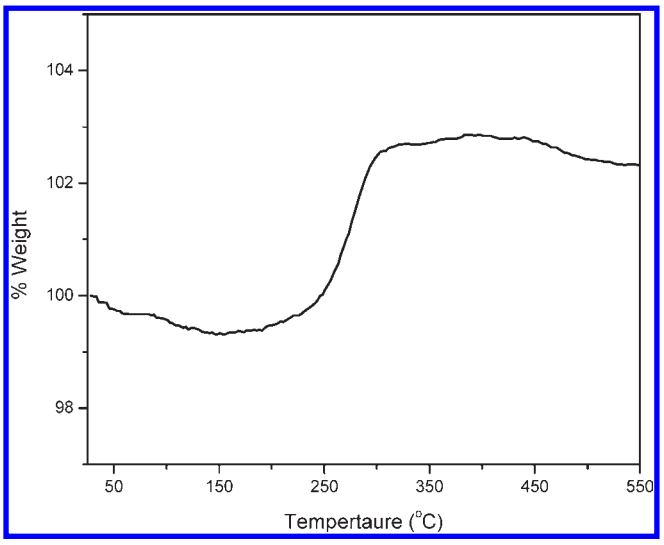

Figure 6. TG curve of $CeScO_3$.

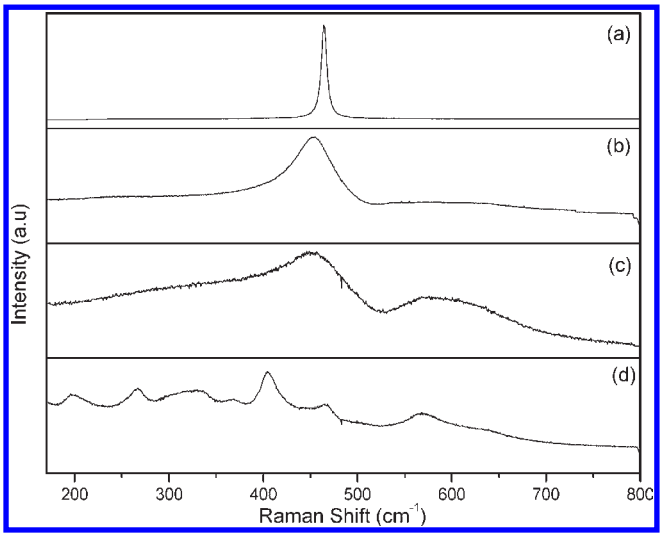

Figure 7. Raman spectra of (a) bulk CeO_2, (b) nano-CeO_2, (c) $Ce_{0.5}Sc_{0.5}O_{1.75}$ solid solution, and (d) $CeScO_3$ perovskite.

nature of the compound. The Raman spectra of $Ce_{0.5}Sc_{0.5}O_{1.75}$ also shows a peak at around 451 cm^{-1} which is a signature of the F-type cubic structure[17] of CeO_2. The hump around 580 cm^{-1} is a characteristic of heavily trivalent ion (Sc^{3+}) substituted CeO_2 lattice.[22,23] It may be noted that the Raman spectra of undoped Sc_2O_3[17] shows a band ~420 cm^{-1}. The product $Ce_{0.5}Sc_{0.5}O_{1.75}$ does not show any peak at this position. These observations clearly indicate that $Ce_{0.5}Sc_{0.5}O_{1.75}$ is a F-type solid solution. On the other hand, the reduced sample, i.e. $CeScO_3$, exhibited the characteristic modes observed in a typical perovskite structure.[24]

Photoluminescence measurement of $CeScO_3$ and $CeScO_3$ doped with 2 mol % Tb^{3+} samples was carried out at room temperature (Figure 8). $CeScO_3$ was excited by a

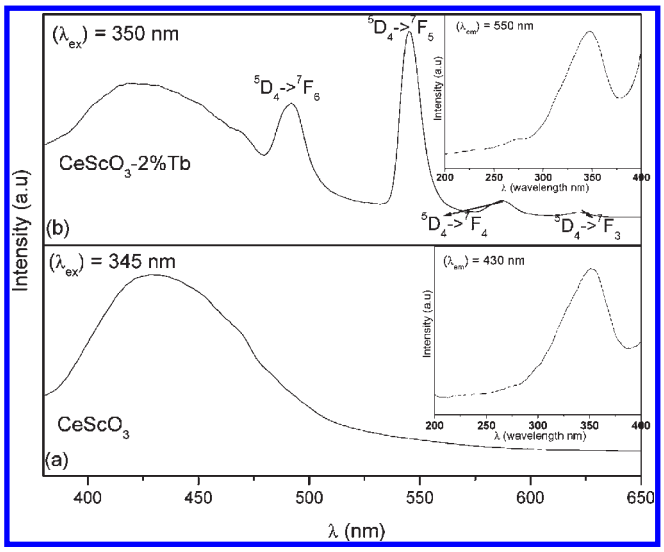

Figure 8. Photoluminescence spectra of $CeScO_3$ and a 2% Tb^{3+} ion doped $CeScO_3$ sample. The inset gives the excitation spectra.

wavelength of 345 nm. The broad peak in the excitation spectra (inset of Figure 8a) over the range of 300−370 nm and centered around 345 nm is characteristic of the 4f → 5d transition of Ce^{3+} ions. It resulted in a broad blue emission centered around 430 nm. $CeScO_3$ doped with 2 mol % Tb^{3+} was excited by 350 nm (inset Figure 8b). The intensity of the broad emission due to the Ce^{3+} host has been reduced considerably, which is attributed to an energy transfer from the Ce^{3+} to Tb^{3+} ion. The strong emission at 545 nm is characteristic of a $^5D_4 \rightarrow {}^7F_5$ transition of Tb^{3+}. It may be noted that the Tb^{3+} ion in general gives a weak emission upon direct excitation due to weak oscillator strength, but in this case, the strong emission due to Tb^{3+} confirms the energy transfer from Ce^{3+} to the guest ion. Some residual blue emission in Tb^{3+} doped $CeScO_3$ reveals an incomplete energy transfer between the the Ce^{3+} and Tb^{3+} ions. These results suggest that $CeScO_3$ could be a potential blue light emitting material for various optical applications when doped with other rare earth ions.

The optical band gap of $CeScO_3$ was measured by a DR-UV−visible spectrophotometer in the reflectance mode. The plot of square of absorbance versus the wavelength is shown as Figure 9. The sample shows an absorbance around 389 nm, which corresponds to an optical band gap of 3.2 eV and in turn reveals the semiconducting nature of this compound. It may be noted that most of the rare earth scandates have their band gap in the range of 5.5−6.5 eV.[1]

3.4. Theoretical Calculation. To understand the reason behind this unusually low band gap of $CeScO_3$, PAW potential plane-wave-based DFT calculations on $CeScO_3$ (*Pnma*) were performed using the generalized gradient approximations (GGA) for the exchange-correlation potential, as parametrized by Perdew−Burke−Ernzerhof.[25] The "Vienna ab initio simulation package" (VASP)[26,27] was used, which solves the Kohn−Sham equations using a plane wave expansion for the valence electron density

(22) Mandal, B. P.; Grover, V.; Roy, M.; Tyagi, A. K. *J. Am. Ceram. Soc.* **2007**, *90*, 2961.
(23) Mandal, B. P.; Roy, M.; Grover, V.; Tyagi, A. K. *J. Appl. Phys.* **2008**, *103*, 033506.
(24) Granado, E.; Moreno, N. O.; Garcý'a, A.; Sanjurjo, J. A.; Rettori, C.; Torriani, I.; Oseroff, S. B.; Neumeier, J. J.; Mcclellan, K. J.; Cheong, S.-W.; Tokura, Y. *Phys. Rev. B* **1998**, *58*, 11435.
(25) Perdew, J. P.; Burke, K.; Wang, Y. *Phys. Rev. B* **1996**, *54*, 16533.
(26) Kresse, G.; Furthmüller, J. *Comput. Mat. Sc.* **1996**, *6*, 15.
(27) Kresse, G.; Furthmüller *Phys. Rev. B* **1996**, *54*, 11169.

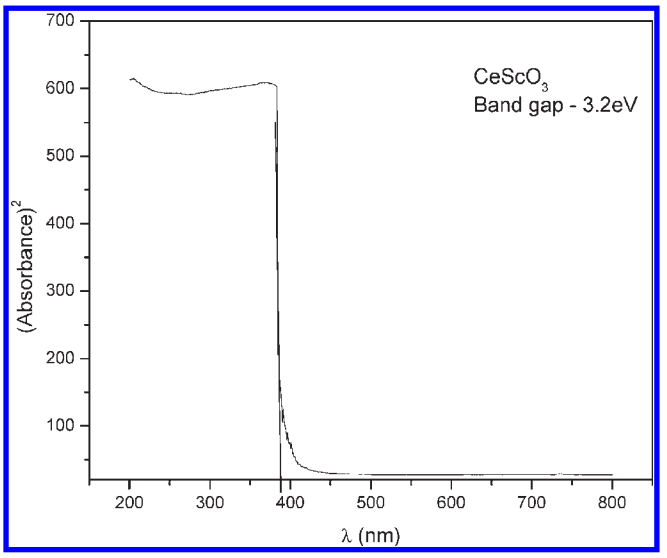

Figure 9. Plot of square of absorbance vs wavelength of the $CeScO_3$ sample.

and wave functions. The interactions between the ions and electrons are described by the "projector augmented wave" (PAW) potentials,[28,29] which use smaller radial cutoffs (core radii) and reconstruct the exact valence wave function with all nodes in the core region. The PAW potentials used in this study are those provided in the VASP database (version 4.6). For Sc, we treated 3p, 4s, and 3d as valence states; while for O, the standard PAW potential was used with s2p4 as valence states. For Ce, we used the "Ce_3" potential which corresponds to trivalent Ce. Our calculations were fully converged with respect to the size of the basis set (kinetic energy cutoff (E_cutoff = 400 eV) and the number of **k**-points (IBZ = 18) for $CeScO_3$. The equilibrium volume was calculated to be 273.53 $Å^3$ (with lattice parameters: a = 5.7220 Å, b = 5.8582 Å, and c = 8.1601 Å) which agrees well with the experimental value of 262.34 $Å^3$. In Figures 10 and 11, plots of total and site- and *l*-projected density of states (DOS) for $CeScO_3$ are shown. As can be seen from the total DOS, the Fermi energy lies close to the high energy end of the valence band which is not fully occupied, giving the structure a semblance of weak metallic character. The total DOS exhibits a band gap of about 3.8 eV between the valence and conduction bands. It must be noted that DFT always overestimates the band gaps; therefore, the above value may be considered as the upper bound to the actual band gap. The partial site- and *l*-projected DOS clearly show that the valence band predominantly has a mixing of O p, Sc d, and Ce d states with small contributions coming from Ce f and Sc p states. The conduction band is mainly dominated by Sc d and Ce d states. The (origin of) band gap in $CeScO_3$ is coming mainly from O p states in the valence band and Sc d (along with Ce d) states in the conduction band, as expected from this rare earth scandate. The d states have energy levels

(28) Blöchl, P. E. *Phys. Rev. B* **1994**, *50*, 17953.
(29) Kresse, G.; Joubert, J. *Phys. Rev. B* **1999**, *59*, 1758.

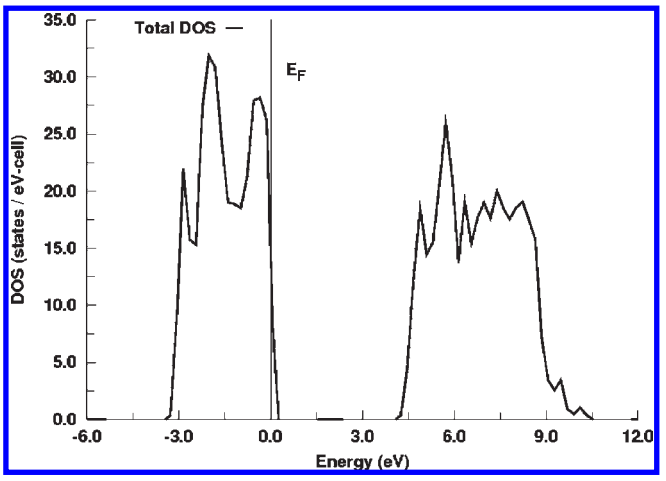

Figure 10. Plot of total DOS for $CeScO_3$.

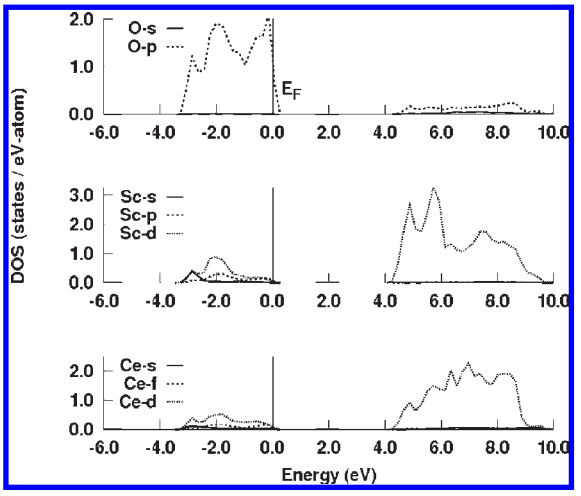

Figure 11. Site- and *l*-projected partial DOS for $CeScO_3$.

with respect to the valence band that scale with their respective d-state energies. The larger the d-state binding energy with respect to vacuum, the closer these d states lie to the oxygen atom derived valence band states and the smaller is the band gap.

4. Conclusion

$CeScO_3$ could be synthesized by a two-step method involving combustion synthesis followed by a vacuum heating in presence of Zr sponge which acts as an oxygen getter. After the first step, a fluorite-type solid solution has been obtained which shows 50 mol % solubility of Sc_2O_3 in CeO_2. Only by a redox reaction was a reversible transformation between fluorite type structure and perovskites structure observed. $CeScO_3$ was found to be a semiconducting oxide with a band gap of 3.2 eV. Photoluminescence measurement revealed that $CeScO_3$ is a potential host material emitting broad blue emission. It was demonstrated that $CeScO_3$ doped with 2% Tb^{3+} ion is an efficient green light emitting material.